magnetochemistry

MDPI

Article

Charge Ordering Transitions of the New Organic Conductors δ_m- and δ_o-(BEDT-TTF)$_2$TaF$_6$

Tadashi Kawamoto [1,*], Kohei Kurata [2], Takehiko Mori [1,3] and Reiji Kumai [4]

1 Department of Materials Science and Engineering, Tokyo Institute of Technology, Tokyo 152-8552, Japan; mori.t.ae@m.titech.ac.jp
2 Department of Organic and Polymeric Materials, Tokyo Institute of Technology, Tokyo 152-8552, Japan; kohei.kurata@outlook.com
3 ACT-C JST, Honcho, Kawaguchi, Saitama 332-0012, Japan
4 Condensed Matter Research Center and Photon Factory, Institute of Materials Structure Science, High Energy Accelerator Research Organization (KEK), Tsukuba, Ibaraki 305-0801, Japan; reiji.kumai@kek.jp
* Correspondence: kawamoto@o.cc.titech.ac.jp; Tel.: +81-3-5734-3657

Academic Editor: Manuel Almeida
Received: 13 January 2017; Accepted: 22 February 2017; Published: 1 March 2017

Abstract: Structural, transport, and magnetic properties of new organic conductors composed of (BEDT-TTF)$_2$TaF$_6$, where BEDT-TTF is bis(ethylenedithio)tetrathiafulvalene, have been investigated. Two δ-type polymorphs, monoclinic and orthorhombic phases are obtained by the electrocrystallization. Both phases show a semiconductor-insulator phase transition at 276 K and 300 K for the monoclinic and orthorhombic phases, respectively; the ground state of both salts is a nonmagnetic insulating state. The low-temperature X-ray diffraction measurements show two-fold superlattice reflections in the intercolumnar direction. The low-temperature crystal structures show a clear charge ordered state, which is demonstrated by the molecular shape and intramolecular bond lengths. The observed checkerboard charge ordered state is in agreement with the charge ordering in a dimer Mott insulator. If we distinguish between the monoclinic and orthorhombic phases, the transition temperature of the δ-type (BEDT-TTF)$_2M$F$_6$ conductors (M = P, As, Sb, and Ta) increases continuously with increasing the anion volume.

Keywords: molecular conductor; electronic correlation; charge order

1. Introduction

Among molecular conductors, bis(ethylenedithio)tetrathiafulvalene (BEDT-TTF) salts with octahedral anions, so-called β-(BEDT-TTF)$_2$PF$_6$ type salts, have a unique arrangement of the donor molecules with a twisted stacking structure (Figure 1) [1–3]. This molecular arrangement is categorized into the δ type; the donor column consists of alternate stacking of two interaction modes: the twisted stacking mode (a1 in Figure 1c) and the parallel stacking mode (a2) slipped along the molecular short axis (ring-over-atom mode) [3]. The highly conducting direction is not the donor stacking direction but the intercolumnar direction [1]. After the discovery of the PF$_6$ salt, several δ-type BEDT-TTF salts with octahedral anions have been developed. The crystal system, however, differs between the PF$_6$ (orthorhombic) and SbF$_6$ (monoclinic) salts despite the same anion shape [4]. The AsF$_6$ salt has been known as a monoclinic compound, but later the orthorhombic crystal has been found [4–7].

The PF$_6$ salt has been investigated using X-ray diffraction and Raman spectra; the phase transition at around room temperature is not a $2k_F$ charge-density-wave but a charge order [8,9]. The charge ordering transition is due to the nearest neighbor Coulomb repulsion V [10–12]. The orthorhombic AsF$_6$ salt also shows a similar charge order to that of the PF$_6$ salt [8]. The charge order has been observed in both the monoclinic AsF$_6$ and SbF$_6$ salts using Raman spectra [13]. Although many

investigations of the δ-type BEDT-TTF salts with octahedral anions have been carried out, the charge ordering transition temperature does not seem to change in the sequence of the anion volume.

In order to clarify the relationship between the transition temperature and the anion volume, the TaF_6 salt is prepared; TaF_6 is the largest anion among MF_6 anions (M = P, As, Sb, and Ta) [14]. In the present paper, we report two δ-type polymorphs of the TaF_6 salts, monoclinic (δ_m) and orthorhombic (δ_o) phases. Although both salts show a charge ordering transition, the transition temperature of the orthorhombic phase is higher than that of the monoclinic phase. If we distinguish between the monoclinic and orthorhombic phases in the δ-type (BEDT-TTF)$_2MF_6$ conductors, the transition temperature increases with increasing the anion volume; this indicates that the chemical pressure affects the charge ordering transition temperature.

2. Results

The crystallographic data of both δ_m- and δ_o-(BEDT-TTF)$_2TaF_6$ at 298 K are shown in Table 1. For the monoclinic δ_m phase, we choose the space group $C2/c$. Although unusual space group $I2/c$ has been used in the SbF_6 salt [4], the unit cell transformation $\boldsymbol{a'} = -\boldsymbol{a} - \boldsymbol{c}$ gives the monoclinic angle $\beta' = 93.99(4)^\circ$ and the reported lattice. In the AsF_6 salt, another unit cell transformation gives the reported $A2/a$ lattice [5]. The orthorhombic δ_o-TaF_6 salt and the PF_6 salt are isostructural, and the space group is $Pnna$. The unit cell volume of the monoclinic phase is slightly larger than that of the orthorhombic phase.

Table 1. Crystallographic data of the (BEDT-TTF)$_2TaF_6$ salts.

	δ_m Phase		δ_o Phase	
Formula	$C_{20}H_{16}S_{16}TaF_6$			
Formula weight	1064.24			
Temperature (K)	298	171	298	39
Crystal system	Monoclinic	Monoclinic	Orthorhombic	Monoclinic
Space group	$C2/c$	$P2_1/n$	$Pnna$	$P2/c$
a (Å)	35.825(12)	35.6108(6)	14.924(9)	13.2594(5)
b (Å)	6.679(4)	13.2887(2)	33.366(14)	14.5036(4)
c (Å)	14.953(8)	14.7148(3)	6.656(2)	33.8724(7)
β (deg)	110.62(3)	110.1387(8)	–	101.206(2)
V (Å^3)	3349(3)	6537.7(2)	3315(3)	6389.8(3)
Z	4	8	4	8
Total reflections	4877	11899	2921	27208
Reflections [$F^2 > 2\sigma(F^2)$]	3571	7889	1558	20909
$R1$ [$F^2 > 2\sigma(F^2)$]	0.0327	0.0818	0.0748	0.1387
$wR2$ (all reflections)	0.0944	0.2172	0.2498	0.3242
GOF	1.028	1.128	1.026	1.231

Figure 1a–d show the crystal structure of the TaF_6 salts. These two phases take similar δ-type structures. For the monoclinic phase, the BEDT-TTF molecular planes of the adjacent conducting layers along the a-axis are almost parallel to each other (Figure 1a). In the orthorhombic phase, however, donor planes are inclined alternately along the interlayer direction (Figure 1b). There is one crystallographically independent donor and a half anion, and a unit cell contains eight donors and four anions, affording the donor to anion ratio 2:1. The terminal donor ethylene-groups are disordered. The donors form a stack along the c-axis for the δ_m phase (a-axis for the δ_o phase) with the twisted mode $a1$ and the ring-over-atom mode $a2$. For the $a1$ mode, the interplanar distance is $d_\perp = 3.58$ Å and the twist angle is $\omega = 29.9^\circ$ in the δ_m phase, and $d_\perp = 3.57$ Å and $\omega = 29.9^\circ$ in the δ_o phase. For the $a2$ mode, the slip distance along the molecular short axis is $d_s = 2.00$ Å, and $d_\perp = 3.67$ Å in the δ_m phase. These values are $d_s = 2.02$ Å and $d_\perp = 3.67$ Å in the δ_o phase.

An anion is located on an inversion center for the δ_m phase. In the δ_o phase, an anion is on a two-fold rotation axis parallel to the a-axis, and fluorine atoms are on general positions.

The arrangement of anions is an isosceles triangle on an anion layer parallel to the *bc*-plane (*ac*-plane) in the δ_m (δ_o) phase. An interaction between the donor hydrogen and anion fluorine atoms shorter than the sum of the van der Waals radii (2.67 Å) [15], a so-called hydrogen bond, is found. Although both terminal ethylene groups of the donor have hydrogen bonds in the δ_o phase, one side terminal of the donor has a hydrogen bond in the δ_m phase. This is due to the difference of the unit cell volumes because the unit cell of the δ_o phase is smaller than that of the δ_m phase.

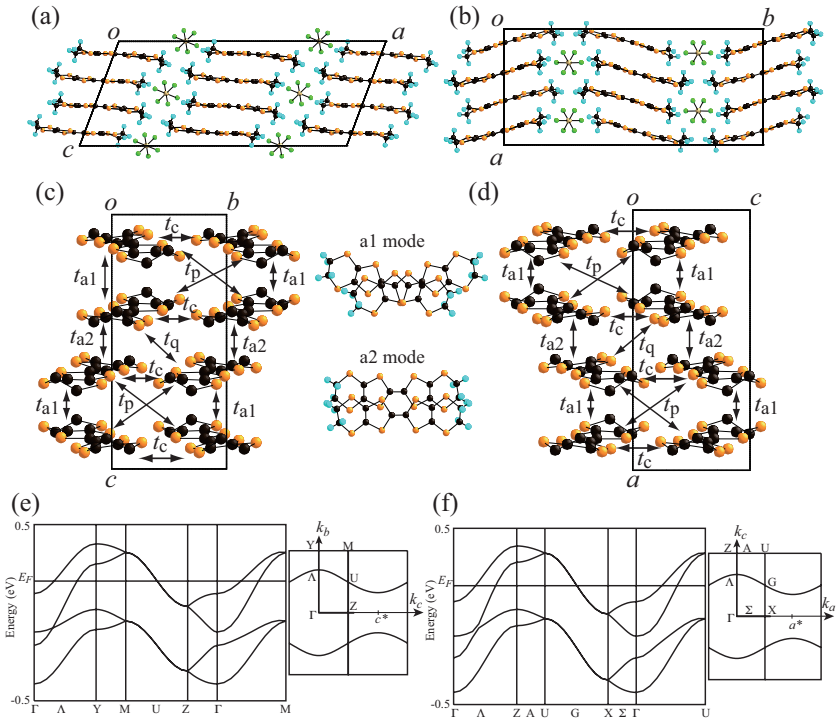

Figure 1. Crystal structure of δ_m-(BEDT-TTF)$_2$TaF$_6$ (**a**) and the δ_o phase (**b**) projected approximately along the molecular short axis. The donor layer of the δ_m phase (**c**) and the δ_o phase (**d**) projected approximately along the molecular long axis. The energy band structure and the Fermi surface of the δ_m phase (**e**) and the δ_o phase (**f**).

The calculated transfer integrals, the distance between the molecular centers R, and the twist angles ω are shown in Table 2. All interaction modes (c, $a1$, $a2$, p, and q) are the same as those of β-(BEDT-TTF)$_2$PF$_6$ [2,3]. The transfer integral of the twisted interaction mode t_{a1} is larger than that of the ring-over-atom mode t_{a2}; this twisted dimer structure is characteristic of this structure. The transverse interactions are large, and t_q is larger than t_{a1}. The energy band structure and Fermi surface are shown in Figure 1e,f. The quasi-one-dimensional Fermi surface is shown in an extended zone scheme because the energy bands degenerate at the zone boundary owing to the crystallographic symmetries.

Figure 2 shows the temperature dependence of the electrical resistivity. Both salts exhibit semiconducting behavior in the measurement temperature region, and show anomaly at approximately 300 K. The phase transition temperature T_c is determined from the peak of $d(\ln \rho)/d(1/T)$ at $T_c = 276$ K and $T_c = 300$ K for the δ_m and δ_o phases, respectively. As shown in the inset of Figure 2, the charge activation energy Δ_{charge} is estimated as 27 and 46 meV for the δ_m and δ_o phases, respectively.

Table 2. Transfer integrals and geometrical parameters of the δ-type $(BEDT\text{-}TTF)_2TaF_6$ salts.

Interaction Mode	t (meV)	R (Å)	ω (deg)
δ_m phase			
c	−75.6	6.68	
$a1$	−103.3	4.49	29.9
$a2$	38.4	4.18	
p	−23.8	8.05	
q	−147.8	5.72	
δ_o phase			
c	−79.4	6.66	
$a1$	−95.9	4.51	29.9
$a2$	37.1	4.19	
p	−24.5	8.04	
q	−141.2	5.72	

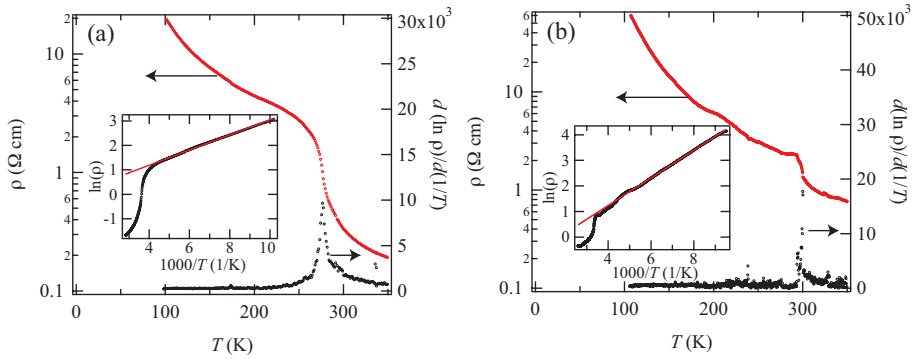

Figure 2. Temperature dependence of the resistivity of the δ_m phase (**a**) and the δ_o phase (**b**). The insets show the Arrhenius plots, and solid lines in the insets are fits to the data.

The Seebeck coefficient of the δ_m phase shows metallic behavior around 300 K, and has anomaly at approximately 280 K (Figure 3). For the δ_o phase, the thermopower shows semiconducting behavior even in the high temperature region and has no anomaly at 300 K where the resistivity has an anomaly. The value of the thermopowers around 300 K is approximately 52 μV/K. This large value is not in agreement with the energy band structure, indicating a strongly correlated electronic system [1,2,16,17].

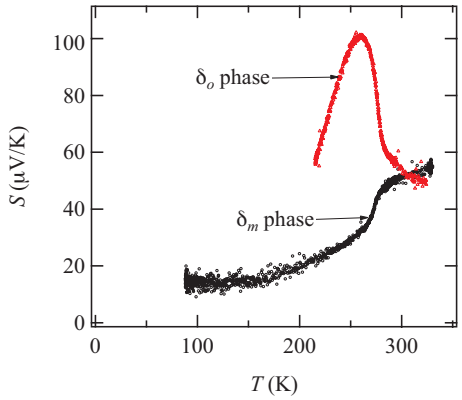

Figure 3. Temperature dependence of Seebeck coefficients of the δ_m and δ_o phases.

Figure 4 shows the temperature dependence of the electron spin resonance (ESR) g-values, peak-to-peak linewidths, and the normalized spin susceptibilities measured under the magnetic field perpendicular to the conducting layers. A single Lorentzian lineshape is observed for both phases.

The spin susceptibility of the δ_m phase clearly decreases below 280 K without a divergent increase of the linewidth, leading to a spin singlet state. The spin susceptibility of the δ_o phase gradually decreases with decreasing temperature, and the spin singlet state appears at low temperatures. However, the phase transition temperature is not clear. The g-values are almost independent of the temperature around the phase transition temperature. The spin activation energy Δ_{spin} is estimated from the simple singlet–triplet model given by $\chi_{spin} \propto (1/T)\exp(-\Delta_{spin}/T)$ in the 100–200 K range. The spin activation energy Δ_{spin} is about 30 meV. Δ_{spin} is in rough agreement with Δ_{charge} estimated from the electrical resistivity.

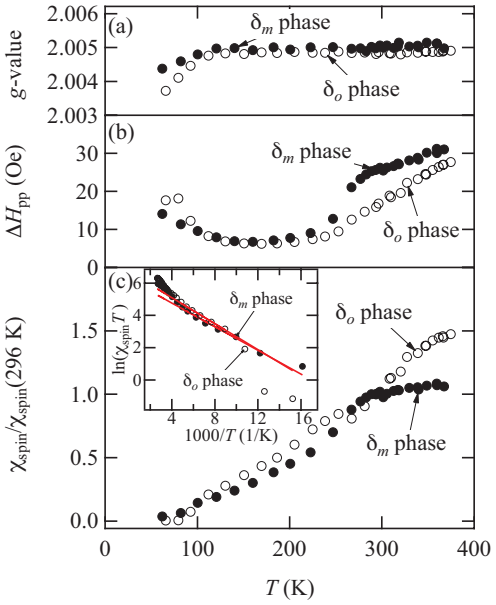

Figure 4. Temperature dependence of ESR g-values (**a**), linewidths (**b**), and the relative spin susceptibilities (**c**) of the δ_m and δ_o phases. The applied magnetic field is perpendicular to the conducting layer for both compounds. The inset shows the Arrhenius plots, and solid lines in the inset are fits to the data.

In order to clarify the origin of the phase transition, the low-temperature X-ray diffraction measurements were performed. Figure 5 shows the X-ray oscillation photographs of both δ_m and δ_o phases. At 171 K, superlattice reflections with the wave vector $\boldsymbol{q_m} = (0, 1/2, 0)$ are observed for the δ_m phase (Figure 5a,b). Although the superlattice reflections are observed at 171 K for the δ_o phase, the wave vector is $\boldsymbol{q_o} = (0, 1/2, 1/2)$ (Figure 5c,d). Figure 6 shows the temperature dependence of the integrated intensity of the superlattice reflections. The superlattice reflection disappears at 277 K and 302 K for the δ_m and δ_o phases, respectively. These results indicate that the temperatures at which the resistivity shows anomaly are the phase transition temperatures.

Figure 7a,b show the crystal structure of the δ_m phase at 171 K. The C-centered unit cell changes to a primitive cell with the space group $P2_1/n$ as shown in Table 1, which is a sub-group of $C2/c$; the superlattice unit cell is $\boldsymbol{a'} = \boldsymbol{a}$, $\boldsymbol{b'} = 2\boldsymbol{b}$, and $\boldsymbol{c'} = \boldsymbol{c}$ because superlattice reflections with $h + k \neq 2n$ appear for hkl, where n is an integer. Some reflections with $h + l \neq 2n$ are observed in $h0l$ reflections. However, in order to analyze the low-temperature average structure, we have chosen $P2_1/n$, because a centrosymmetric space group has been suggested by SHELXT; the program SHELXT proposes possible space groups on the basis of phases in the space group $P1$ without using systematic absences [18]. In the present space group, there are four crystallographic independent molecules along the stacking direction (Figure 7a). The molecules in the nearest neighbor columns in the conducting sheet is connected by a two-fold screw axis; this indicates that the charge ordering pattern is not related by the glide symmetry. Moreover, in the case of $P2_1$, the maximum shift/error for the parameter

refinement does not converge, and the atomic coordinates of four additional independent molecules are connected by the inversion symmetry operation. Although the existence of the inversion center is important for electronic polarity, we do not treat this problem further in the present work.

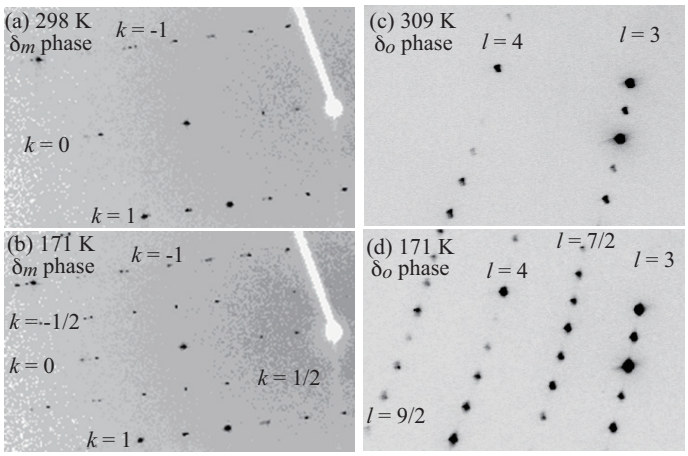

Figure 5. X-ray oscillation photographs of the δ_m phase at 298 K (**a**) and 171 K (**b**), and of the δ_o phase at 309 K (**c**) and 171 K (**d**).

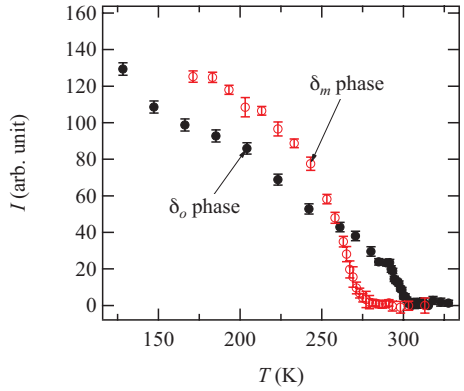

Figure 6. Temperature dependence of the integrated intensity of superlattice reflections. The background intensities are subtracted. Although integrated intensity is measured using a four circle diffractometer for the δ_o phase, this is measured using an imaging plate for the δ_m phase. The indices of the used reflections are $4, -1/2, -3$ for the δ_m phase, and $8, -3/2, -1/2$ for the δ_o phase.

Figure 7c,d show the crystal structure of the δ_o phase at 39 K. Some reflections with $l \neq 2n$ for $h0l$ are observed. However, we have chosen $P2/c$ as suggested by SHELXT owing to the same reason as the δ_m phase (Table 1). This space group is a sub-group of $Pnna$, where the superlattice is given by $\boldsymbol{a'} = 2\boldsymbol{c}$, $\boldsymbol{b'} = \boldsymbol{a}$, and $\boldsymbol{c'} = -\boldsymbol{c} - \boldsymbol{b}$ on the basis of the superlattice wave vector $\boldsymbol{q_o} = (0, 1/2, 1/2)$. The n-glide in the original cell corresponds to the c-glide in the new unit cell. In the δ_o phase, molecules in the nearest neighbor column in the conducting sheet are related by the inversion symmetry. If the space group has no inversion center ($P2$), the nearest neighbor column is composed of four other independent molecules. However, in the case of $P2$, the analysis does not converge similarly to $P2_1$ in the δ_m phase.

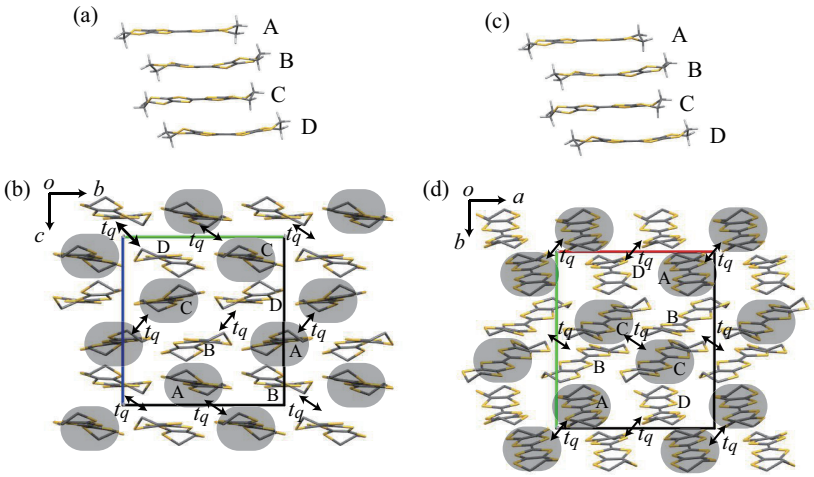

Figure 7. Crystal structure of the δ_m phase at 171 K (**a**,**b**) and of the δ_o phase at 39 K (**c**,**d**). Four crystallographically independent molecules (A, B, C, and D) exist for both phases (**a**,**c**). A and C (B and D) molecules are flat (bent). Black rounded rectangles denote hole-rich molecules, and t_q is the interaction mode q in the high temperature structure (**b**,**d**).

A terminal ethylene group at one side is disordered except for the D molecule in the δ_m phase. The A and C molecules are disordered in the δ_o phase. The completely ordered structure has been observed in the PF_6 and δ_o-AsF_6 salts. However, this conformational ordering depends on the cooling speed [8]. The cooling speed approximately 1–3 K/min is too fast to attain a completely ordered structure. Although A and C molecules are flat, B and D molecules are bent for both δ_m and δ_o phases (Figure 7a,c); the bent TTF skeleton is characteristic of the neutral BEDT-TTF molecule [19]. The BEDT-TTF molecules have a boat-like structure. The dihedral angles between the central and outer tetrathio-substituted ethylene moieties are approximately 2.4°–3.0° in the A and C molecules. These are approximately 8.5°–13.7° in the B and D molecules in the δ_m phase, and 7.0°–10.9° in the δ_o phase. This clearly shows that the low-temperature phase is a charge ordered state. The charges of the BEDT-TTF molecules are estimated empirically from the bond lengths [20]: $Q_A = +0.8(1)$, $Q_B = +0.1(1)$, $Q_C = +0.6(1)$, and $Q_D = -0.1(1)$ in the δ_m phase. In the δ_o phase, the charges are $Q_A = +0.8(2)$, $Q_B = +0.5(2)$, $Q_C = +0.7(2)$, and $Q_D = +0.2(2)$. The estimated Q values are in agreement with the molecular shape; the flat A and C molecules are hole rich, whereas the bent B and C molecules are nearly neutral. The calculated energy levels of the highest occupied molecular orbital (HOMO) of these molecules show that the averaged HOMO level of the bent molecules is lower than that of the flat molecules by ∼0.1 eV. This is in agreement with the charge disproportionation between the flat and bent molecules. The hole-rich donor molecules are connected by the transfer integral t_q with the largest absolute value in the high temperature structure (Figure 7b,d); then, a spin-singlet state is realized. Although A and C molecules are connected in the δ_m phase ($R_q^{AC} = 5.71$ Å), A and A or C and C molecules are connected in the δ_o phase ($R_q^{AA} \approx R_q^{CC} = 5.70$ Å). The absolute value of the transfer integral between A and C molecules $|t_q^{AC}|$ increases (174.7 meV), but $|t_q^{BD}|$ decreases (114.1 meV) despite $R_q^{BD} < R_q^{AC}$ in the δ_m phase. This is due to the molecular shape; B and D molecules are bent. The side-by-side molecular center distance is slightly modulated; the averaged difference is approximately 0.10 Å. These tendencies are the same as those in the δ_o phase. The anion arrangement is also changed; the isosceles triangle pattern is deformed. There are many hydrogen bonds between the donors and anions in the low-temperature structure. The short hydrogen bonds (≤2.50 Å) are observed in the B and D molecules for both phases.

3. Discussion

The difference between the δ_m and δ_o phases is the inclination of the donor plane in a conducting layer. In the δ_o phase, the plane inclination changes alternately along the normal direction to the conducting layer. The same difference is found in the AsF_6 salts, which indicates that the monoclinic phase of the AsF_6 salt differs from the orthorhombic phase discovered by Senadeera et al. [4–7]. Nogami et al. have confirmed the lattice constants of the orthorhombic phase of the AsF_6 salt and solved the structure at 110 K including the superlattice reflections; the superlattice unit cells of both δ_o-PF_6 and δ_o-AsF_6 salts are also orthorhombic [8]. Leung et al. have found two-fold superlattice reflections in the monoclinic AsF_6 salt above 125 K, where the wave vector $\boldsymbol{b}^*/2$ is the same as that of the δ_m-TaF_6 salt. The Raman spectra of the monoclinic AsF_6 salt show the charge ordering at approximately 260 K [13]. Therefore, we have to distinguish between the monoclinic and orthorhombic phases in the AsF_6 salts; the charge ordering transition temperatures are $T_c = 264$ K and 298 K for the monoclinic and orthorhombic phases, respectively. The transition temperature T_c of the orthorhombic phases is generally higher than that of the monoclinic phases in the other δ-type (BEDT-TTF)$_2MF_6$ salts as shown in Table 3. If we distinguish the crystal system, the transition temperature increases independently with increasing the anion size (Figure 8). This is in agreement with the concept of chemical pressure; the smaller the anion volume, the higher the pressure region. Actually, the transition temperature decreases with increasing the external pressure in the PF_6 salt [6].

Table 3. Summary of the δ-type (BEDT-TTF)$_2MF_6$ salts.

	δ_m-PF_6	δ_o-PF_6	δ_m-AsF_6	δ_o-AsF_6	δ_m-SbF_6	δ_o-SbF_6	δ_m-TaF_6	δ_o-TaF_6
existence	[b]	yes	yes	yes	yes	[b]	yes	yes
spin singlet	–	yes	yes	yes	yes	–	yes	yes
superlattice [a]	–	$\boldsymbol{c}^*/2$	$\boldsymbol{b}^*/2$	$\boldsymbol{c}^*/2$	[b]	–	$\boldsymbol{b}^*/2$	$\boldsymbol{b}^*/2+\boldsymbol{c}^*/2$
charge ordering	–	yes	yes	yes	yes	–	yes	yes
T_c (K)	–	297	264	∼ 298 [c]	273	–	276	300
Ref.	–	[1,6,8,9]	[4,5,13]	[6,8]	[4,13]	–	[d]	[d]

[a] For the δ_m-AsF_6 salt, the unit cell is transformed to that of the TaF_6 salt, $C2/c$; [b] unknown; [c] T_c is estimated from the temperature dependence of the superlattice reflection in Ref. [6]; [d] present work.

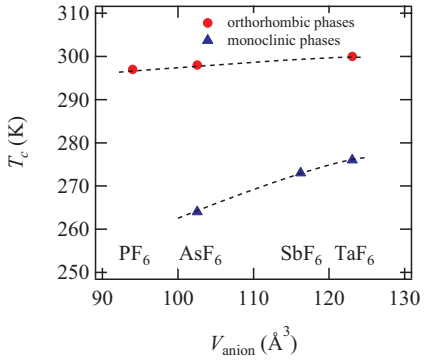

Figure 8. Anion volume dependence of the charge ordering temperature of δ-type (BEDT-TTF)$_2MF_6$ (M = P, As, Sb, and Ta). Anion volumes are estimated using Figure 2 in Ref. [14]. Dashed lines are guides to the eye.

The relationship between the charge order and anion has been investigated in α-(BEDT-TTF)$_2I_3$ [21]. The hydrogen bonds of the hole-rich donors are shorter than those of the hole-poor donors in α-(BEDT-TTF)$_2I_3$; the hydrogen bonds between the donors and anions affect the charge ordering transition. In the present compounds, however, the donors with short hydrogen bonds are hole poor molecules, i.e., bent neutral molecules. This indicates that the anion shift does

not affect the present phase transition. Moreover, the shift of the donors is also small; this molecular displacement is known as a bond order wave [22,23]. The slight displacement is not dominant in the phase transition that leads to the charge ordered state. The above results show that the origin of the phase transition is due to the electronic correlation between the donor molecules.

The experimentally obtained charge ordered pattern is estimated from the high temperature crystal structure. In the θ-type BEDT-TTF compounds, theoretical investigation has revealed several charge ordering patterns depending on t/V, which have been verified by different kinds of experiments [10–12]. However, a simple method to expect the charge ordering pattern has been proposed, since the point charge approximation is appropriate; V is proportional to $1/R$ for $R \geq 4$ Å, where R is the distance between the molecular centers [24]. Table 4 shows the transfer integrals and intermolecular distances in the high temperature structure. This shows a trend for the molecular center distances ($R_{a2} < R_{a1} < R_q < R_c < R_p$), and $1/R_{a1} \sim 1/R_{a2}$. Therefore, we use V_a as the stacking direction V and others (V_q, V_c, and V_p) to calculate the potential energy for several charge ordering patterns by the point charge approximation (Figure 9).

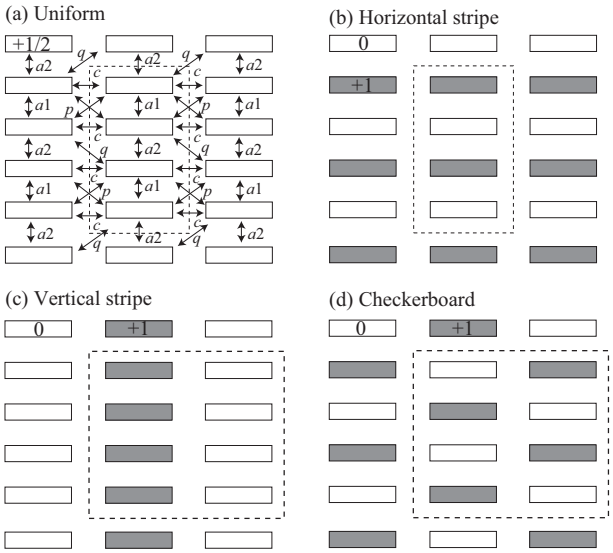

Figure 9. Charge order patterns of the δ-type salts. (**a**) uniform; (**b**) horizontal stripe; (**c**) vertical stripe; and (**d**) checkerboard. The dashed line shows a unit cell.

The extended Hubbard model is written as follows [10,12]:

$$H = -\sum_{\langle ij\rangle\sigma}(t_{ij}c^{\dagger}_{i\sigma}c_{j\sigma} + \text{h.c.}) + \sum_{i} U n_{i\uparrow}n_{i\downarrow} + \sum_{\langle ij\rangle} V_{ij}n_i n_j, \quad (1)$$

where $\langle ij\rangle$ denotes pairs of the lattice sites i and j, $c^{\dagger}_{i\sigma}(c_{i\sigma})$ is the creation (annihilation) operator for a hole with spin $\sigma(=\uparrow,\downarrow)$ at the i site, and $n_{i\sigma} = c^{\dagger}_{i\sigma}c_{i\sigma}$ is the number operator with $n_i = n_{i\uparrow} + n_{i\downarrow}$. U is the onsite Coulomb repulsion, and t_{ij} and V_{ij} are the transfer integral and the nearest neighbor Coulomb repulsion between sites i and j. We neglect t_{ij} and assume the static limit in order to investigate complicated charge-order patterns [24–26]. The static-limit potential energies are listed in Table 5. The ratios $V_p/V_a = R_a/R_p \sim 0.54$, $V_c/V_a \sim 0.65$, and $V_q/V_a \sim 0.76$ give the energies on the right side (V_a energy) in Table 5. Since V_a is much larger than other Vs, the vertical pattern is unlikely. However, because of $V_c \leq V_q$, the horizontal pattern is more stable than the checkerboard in disagreement with the experiments. The checkerboard pattern is most stable when V_a and V_c make a square lattice [27]. Although V_a is obviously large, the relative importance of V_c and V_q is less clear. These stripe patterns have very close static energies, and the point charge approximation is insufficient to distinguish the stability of different stripe patterns. This is also in the case of β-(*meso*-DMBEDT-TTF)$_2$PF$_6$ with the checkerboard charge

ordering, where DMBEDT-TTF stands for 2-(5,6-dihydro-1,3-dithiolo[4,5-b][1,4]dithiin-2-ylidene)-5,6-dihydro-5,6-dimethyl-1,3-dithiolo[4,5-b][1,4]dithiin [26,28].

Table 4. Transfer integrals and geometrical parameters of the δ-type $(BEDT\text{-}TTF)_2AsF_6$ and $(BEDT\text{-}TTF)_2PF_6$ salts.

Interaction Mode	t (meV)	R (Å)	ω (deg)
δ_m-AsF_6 [a]			
c	−77.7	6.67	
$a1$	−109.5	4.45	29.9
$a2$	33.2	4.14	
p	−23.4	8.01	
q	−156.4	5.71	
δ_o-AsF_6 [b]			
c	−74.8	6.69	
$a1$	−98.4	4.50	30.1
$a2$	32.3	4.20	
p	−22.4	8.07	
q	−139.5	5.76	
δ_o-PF_6 (From Ref. [2])			
c	−84	–	
$a1$	−104	–	–
$a2$	32	–	
p	−28	–	
q	−141	–	

[a] The atomic coordinates are in Ref. [5]; [b] The atomic coordinates are in Ref. [7].

Table 5. Potential energies of the charge-ordered patterns per unit cell in the δ-type.

Pattern	V Energy	V_a Energy
Uniform	$E_u = \frac{U}{4} + V_a + V_c + V_p + \frac{V_q}{2}$	$\frac{U}{4} + 2.57V_a$
Horizontal	$E_h = \frac{U}{2} + 2V_c$	$\frac{U}{2} + 1.3V_a$
Vertical	$E_v = \frac{U}{2} + 2V_a$	$\frac{U}{2} + 2V_a$
Checkerboard	$E_c = \frac{U}{2} + 2V_p + V_q$	$\frac{U}{2} + 1.84V_a$

We propose another explanation of the present results. The donor molecules have uniform side-by-side arrangement along the $\boldsymbol{b}$ direction in the δ_m-TaF_6 salt. This direction is the highest conducting direction, and the Fermi surface is perpendicular to the $\boldsymbol{b}^*$ direction (Figure 1c,e). The value of $|t_{a1}|$ is smaller than $|t_q|$, and much smaller than the dimerization in the κ-type BEDT-TTF salts, where the dimer Mott insulating picture is realized ($t_{\mathrm{dimer}} \sim 250$ meV). The molecular center distance $R_{a1} \sim 4.5$ Å is almost the same as that in the dimer of κ-type salts (∼ 4.0 Å). Then, t/V of the $a1$ mode is half of the κ-type salt and comparatively small. However, t/V for q is 90% of that of the κ-type, and the dimerization due to q is important. The energy band in Figure 1 splits into two by taking the oblique dimerization due to q into account. The band splitting has been observed as the inter-band transition in the polarized reflectance spectra of the δ_o-PF_6 salt [29]. The present compounds show semiconducting behaviors even at 350 K sufficiently higher than the phase transition temperature. This indicates that the high temperature phase is a paramagnetic dimer Mott insulator. In the present compounds, a dimer is surrounded by eight neighboring dimers, i.e., a quasi-square lattice, where all dimers have one hole; the dimers are connected by the horizontal interaction composed of two c modes and one $a2$ mode, the vertical $a1$ mode, and the diagonal p mode. The interdimer Coulomb repulsion leads to the checkerboard type charge order $(2, 0, 2, 0)$ because of the relationship $V_p < V_c < V_a$, and the spin singlet state in the dimer is realized. The spin singlet charge ordering has been observed in the dimer Mott insulator κ-$(BEDT\text{-}TTF)_4[Co(CN)_6][N(C_2H_5)_4]\cdot 2H_2O$; the charged dimer composed of hole-rich flat donors and the neutral dimer of bent donors exist in the checkerboard charge ordered state [30].

The wave vector of the superlattice reflection of the δ_o-TaF_6 salt differs from those of other MF_6 salts, but this is only due to the alignment along the interlayer b-axis. The charge ordering transition temperature increases systematically as the transfer integral $|t_q|$ decreases, following a single line both for the monoclinic and orthorhombic phases (Figure 10). R_q is almost the same, and the ratio $|t_q|/V_q$ increases as $|t_q|$ increases. This suggests the importance of the dimerization q [3].

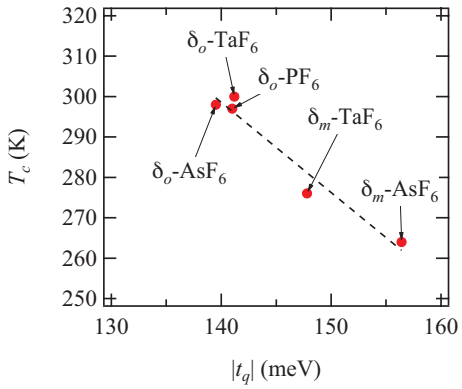

Figure 10. Charge ordering temperatures as a function of $|t_q|$. The dashed line shows linear dependence.

4. Materials and Methods

Single crystals of (BEDT-TTF)$_2$TaF$_6$ were grown by electrocrystallization. The crystal structures were determined by the X-ray single crystal structure analyses. The X-ray diffraction measurements were made on a Rigaku AFC7R four-circle diffractometer (Rigaku Corporation, Tokyo, Japan) with graphite monochromated Mo-$K\alpha$ radiation and a rotating anode generator ($\lambda = 0.71069$ Å). The X-ray oscillation photographs above 170 K were taken using a Rigaku R-AXIS RAPID II imaging plate with Cu-$K\alpha$ radiation from a rotating anode source with a confocal multilayer X-ray mirror (RIGAKU VM-Spider, $\lambda = 1.54187$ Å). For the low-temperature X-ray measurements, the samples were cooled by a nitrogen gas-stream cooling method. Low-temperature X-ray oscillation photographs at 39 K were taken using an imaging plate with Si monochromated synchrotron radiation ($\lambda = 0.99884(2)$ Å) at BL-8B of the Photon Factory, KEK, Tsukuba, Japan; the wavelength was calibrated using CeO_2. The sample was cooled by a helium gas-stream cooling method. The structures were solved by direct methods (SIR2008 and SHELXT) and refined by the full-matrix least-squares procedure (SHELXL) [18,31,32]. Crystallographic data have been deposited with Cambridge Crystallographic Data Center: deposition numbers CCDC 1526712 and 1526713. The energy band structures were calculated on the basis of the molecular orbital calculation and tight-binding approximation [33].

The electrical resistivities were measured by the four-probe method with low-frequency AC current (1.0 μA). Lock-in amplifiers were used for high-sensitivity detection. Thermoelectric power measurements were carried out by the two terminal method [34]. Electron spin resonance (ESR) spectra were measured using a conventional X-band spectrometer (JEOL JES-TE100, Tokyo, Japan). The sweep width of the magnetic field and the g-values were calibrated by the spectra of Mn^{2+}/MgO with a hyperfine structure constant of 86.77 Oe and g_0 of 2.00094. All measurements were performed after examining the lattice parameters using X-ray oscillation photographs.

5. Conclusions

Two polymorphs of (BEDT-TTF)$_2$TaF$_6$ have the same type of δ-type structure, and only the crystal system differs. The present compounds are categorized into a dimer Mott insulator because of the semiconducting behavior even at 350 K. The charge ordering transition is observed at 276 K and 300 K for the monoclinic (δ_m) and the orthorhombic (δ_o) phases, respectively. The bent and flat BEDT-TTF molecules exist in the low-temperature insulting phase, indicating the checkerboard charge ordering. The checkerboard pattern results in a spin singlet state due to the oblique dimerization q mode and the

interdimer Coulomb repulsion. If we distinguish the crystal system, the charge ordering transition temperature increases systematically with increasing of the anion size.

Acknowledgments: This work was partially performed under the approval of the Photon Factory Program Advisory Committee (Proposal No. 2014G089) and supported by Japan Society for the Promotion of Science (JSPS) KAKENHI Grant Numbers 24540364 and 16K05436.

Author Contributions: T.K. and T.M. conceived and designed the experiments; K.K. and T.K. performed the experiments; K.K. and T.K. analyzed the data; R.K. contributed experiment and analysis tools for diffraction measurements using synchrotron radiation; and T.K. and T.M. wrote the paper.

Conflicts of Interest: The authors declare no conflict of interest.

References

1. Kobayashi, H.; Mori, T.; Kato, R.; Kobayashi, A.; Sasaki, Y.; Saito, G.; Inokuchi, H. Transverse conduction and metal-insulator transition in β-(BEDT-TTF)$_2$PF$_6$. *Chem. Lett.* **1983**, *12*, 581–584.
2. Mori, T.; Kobayashi, A.; Sasaki, Y.; Kato, R.; Kobayashi, H. Band structure of β-(BEDT-TTF)$_2$PF$_6$. One-dimensional metal along the side-by-side molecular array. *Solid State Commun.* **1985**, *53*, 627–631.
3. Mori, T. Structural genealogy of BEDT-TTF-based organic conductors III. twisted molecules: δ and α' phases. *Bull. Chem. Soc. Jpn.* **1999**, *72*, 2011–2027.
4. Laversanne, R.; Amiell, J.; Delhaes, P.; Chasseau, D.; Hauw, C. A metal-insulator phase transition close to room temperature: (BEDT-TTF)$_2$SbF$_6$ and (BEDT-TTF)$_2$AsF$_6$. *Solid State Commun.* **1984**, *52*, 177–181.
5. Leung, P.C.; Beno, M.A.; Blackman, G.S.; Coughlin, B.R.; Miderski, C.A.; Joss, W.; Crabtree, G.W.; Williams, J.M. Structure of semiconducting 3,4;3′,4′-bis(ethylenedithio)-2,2′,5,5′-tetrathiafulvalene-hexafluoroarsenate (2:1), (BEDT-TTF)$_2$AsF$_6$, (C$_{10}$H$_8$S$_8$)$_2$AsF$_6$. *Acta Crystallogr. Sect. C* **1984**, *40*, 1331–1334.
6. Senadeera, G.K.R.; Kawamoto, T.; Mori, T.; Yamaura, J.; Enoki, T. $2k_F$ CDW transition in β-(BEDT-TTF)$_2$PF$_6$ family salts. *J. Phys. Soc. Jpn.* **1998**, *67*, 4193–4197.
7. Senadeera, G.K.R. *Report for "33rd International Course for Advanced Research Chemistry and Chemical Engineering"*; Tokyo Tech./United Nations Educational, Scientific and Cultural Organization (UNESCO): Tokyo, Japan, 1998.
8. Nogami, Y.; Mori, T. Unusual $2k_F$ CDW state with enhanced charge ordering in β-(BEDT-TTF)$_2$AsF$_6$ and PF$_6$. *J. Phys. IV Fr.* **2002**, *12*, 233–234.
9. Ding, Y.; Tajima, H. Optical study on the charge ordering in the organic conductor β-(BEDT-TTF)$_2$PF$_6$. *Phys. Rev. B* **2004**, *69*, 115121.
10. Seo, H. Charge ordering in organic ET compounds. *J. Phys. Soc. Jpn.* **2000**, *69*, 805–820.
11. Takahashi, T.; Nogami, Y.; Yakushi, K. Charge ordering in organic conductors. *J. Phys. Soc. Jpn.* **2006**, *75*, 051008.
12. Seo, H.; Merino, J.; Yoshioka, H.; Ogata, M. Theoretical aspects of charge ordering in molecular conductors. *J. Phys. Soc. Jpn.* **2006**, *75*, 051009.
13. Kowalska, A.; Wojciechowski, R.; Ulanski, J. Phase transitions in β-(BEDT-TTF)$_2$$XF_6$ (X = P, Sb or As) salts as seen by Raman spectroscopy. *Mater. Sci. Pol.* **2004**, *22*, 353–358.
14. Williams, J.M.; Beno, M.A.; Sullivan, J.C.; Banovetz, L.M.; Braam, J.M.; Blackman, G.S.; Carlson, C.D.; Greer, D.L.; Loesing, D.M.; Carneiro, K. Role of monovalent anions in organic superconductors. *Phys. Rev. B* **1983**, *28*, 2873–2876.
15. Bondi, A. van der Waals Volumes and Radii. *J. Phys. Chem.* **1964**, *68*, 441–451
16. Chaikin, P.M.; Beni, G. Thermopower in the correlated hopping regime. *Phys. Rev. B* **1976**, *13*, 647–651.
17. Kwak, J.F.; Beni, G. Thermoelectric power of a Hubbard chain with arbitrary electron density: Strong-coupling limit. *Phys. Rev. B* **1976**, *13*, 652–657.
18. Sheldrick, G.M. SHELXT—Integrated space-group and crystal structure determination. *Acta Crystallogr. Sect. A* **2015**, *71*, 3–8.
19. Kobayashi, H.; Kobayashi, A.; Sasaki, Y.; Saito, G.; Inokuchi, H. The crystal and molecular structures of bis(ethylenedithio)tetrathiafulvalene. *Bull. Chem. Soc. Jpn.* **1986**, *59*, 301–302.
20. Guionneau, P.; Kepert, C.J.; Bravic, G.; Chasseau, D.; Truter, M.R.; Kurmoo, M.; Day, P. Determining the charge distribution in BEDT-TTF salts. *Synth. Met.* **1997**, *86*, 1973–1974.

21. Alemany, P.; Pouget, J.P.; Canadell, E. Essential role of anions in the charge ordering transition of α-(BEDT-TTF)$_2$I$_3$. *Phys. Rev. B* **2012**, *85*, 195118.
22. Pouget, J.P. Bond and charge ordering in low-dimensional organic conductors. *Physica B* **2012**, *407*, 1762–1770.
23. Pouget, J.P. Interplay between electronic and structural degrees of freedom in quarter-filled low dimensional conductors. *Physica B* **2015**, *460*, 45–52.
24. Mori, T. Estimation of off-site Coulomb integrals and phase diagrams of charge ordered states in the θ-phase organic conductors. *Bull. Chem. Soc. Jpn.* **2000**, *73*, 2243–2253.
25. Mori, T. Non-stripe charge order in the θ-phase organic conductors. *J. Phys. Soc. Jpn.* **2003**, *72*, 1469–1475.
26. Mori, T. Non-stripe charge order in dimerized organic conductors. *Phys. Rev. B* **2016**, *93*, 245104.
27. Ohta, Y.; Tsutsui, K.; Koshibae, W.; Maekawa, S. Exact-diagonalization study of the Hubbard model with nearest-neighbor repulsion. *Phys. Rev. B* **1994**, *50*, 13594–13602.
28. Kimura, S.; Suzuki, H.; Maejima, T.; Mori, H.; Yamaura, J.; Kakiuchi, T.; Sawa, H.; Moriyama, H. Checkerboard-type charge-ordered state of a pressure-induced superconductor, β-(*meso*-DMBEDT-TTF)$_2$PF$_6$. *J. Am. Chem. Soc.* **2006**, *128*, 1456–1457.
29. Tajima, H.; Yakushi, K.; Kuroda, H.; Saito, G. Polarized reflectance spectrum of β-(BEDT-TTF)$_2$PF$_6$. *Solid State Commun.* **1985**, *56*, 251–254.
30. Ota, A.; Ouahab, L.; Golhen, S.; Yoshida, Y.; Maesato, M.; Saito, G.; Świetlik, R. Phase transition from Mott insulating phase into the charge ordering phase with molecular deformation in charge-transfer salts κ-(ET)$_4$[M(CN)$_6$][N(C$_2$H$_5$)$_4$]·2H$_2$O (M = Co^{III} and Fe^{III}). *Chem. Mater.* **2007**, *19*, 2455–2462.
31. Burla, M.C.; Caliandro, R.; Camalli, M.; Carrozzini, B.; Cascarano, G.L.; Caro, L.D.; Giacovazzo, C.; Polidori, G.; Siliqi, D.; Spagna, R. *IL MILIONE*: A suite of computer programs for crystal structure solution of proteins. *J. Appl. Crystallogr.* **2007**, *40*, 609–613.
32. Sheldrick, G.M. Crystal structure refinement with SHELXL. *Acta Crystallogr. Sect. C* **2015**, *71*, 3–8.
33. Mori, T.; Kobayashi, A.; Sasaki, Y.; Kobayashi, H.; Saito, G.; Inokuchi, H. The intermolecular interaction of tetrathiafulvalene and bis(ethylenedithio)tetrathiafulvalene in organic metals. Calculation of orbital overlaps and models of energy-band structures. *Bull. Chem. Soc. Jpn.* **1984**, *57*, 627–633.
34. Chaikin, P.M.; Kwak, J.F. Apparatus for thermopower measurements on organic conductors. *Rev. Sci. Instrum.* **1975**, *46*, 218–220.